© Indian Academy of Sciences

CrossMark

Synthesis, characterization and electrochemical performance of $Li_2Ni_xFe_{1-x}SiO_4$ cathode materials for lithium ion batteries

A Y SHENOUDA and M M S SANAD*

Central Metallurgical Research and Development Institute (CMRDI), Tebbin, P.O. Box 87 Helwan, Egypt
*Author for correspondence (mustafa_sanad2002@yahoo.com)

Abstract. $Li_2Ni_xFe_{1-x}SiO_4$ ($x = 0$, 0.2, 0.4, 0.6, 0.8 and 1) samples were prepared by a sol–gel process. The crystal structure of prepared samples of $Li_2Ni_xFe_{1-x}SiO_4$ was characterized using an X-ray diffractometer. Different crystallographic parameters such as crystallite size and lattice cell parameters have been calculated. Scanning electron microscopy and Fourier transform infrared spectroscopy investigations were carried out, which reveal the morphology and function groups of the synthesized samples. Furthermore, electrochemical impedance spectra measurements are performed. The obtained results indicated that the highest conductivity is achieved for the $Li_2Ni_{0.4}Fe_{0.6}SiO_4$ electrode compound. It was observed that $Li–Li_2Ni_{0.4}Fe_{0.6}SiO_4$ battery has initial discharge capacity of 164 mAh g^{-1} at 0.1C rate. The cycle life performance of all $Li_2Ni_xFe_{1-x}SiO_4$ batteries ranged between 100 and 156 mAh g^{-1} with coulombic efficiency range between 70.9 and 93.9%.

Keywords. Positive electrodes; lithium metal silicates; electrical conductivity; cyclic performance.

1. Introduction

The rechargeable lithium ion batteries for portable electronic devices (e.g., PC and laptop computers, wireless and mobile phones, camcorders, etc.) have lately shown a strong tendency for expansion [1–4]. Polyanion compounds have been identified as suitable positive materials for most of the lithium ion batteries as they are safer and cheaper than the commonly used lithium transition metal oxides [5,6].

Different from lithium transition metal phosphate, which has only one lithium ion per formula unit [7–9], Li_2MSiO_4 has two lithium ions per formula unit, suggesting a higher theoretical capacity than phosphates. Therefore, it is currently considered as a promising alternative cathode material for lithium-ion batteries [10–13]. However, these orthosilicate cathode materials suffer from the high to low rate capability due to its diffusion-controlled kinetics of the electrochemical process, which is limited by intrinsic poor electronic conductivity.

During the last two decades, lithium transition metal orthosilicates (Li_2MSiO_4, M = V, Cr, Mn, Fe, Co, Ni, etc.) were prepared and characterized as potential cathode materials for lithium ion batteries [14–21]. A previous study in 2010 by Deng *et al* [22] confirmed large difference between the electrochemical behaviours of the Li_2FeSiO_4 and Li_2MnSiO_4 samples prepared by a citric-acid-assisted sol–gel method. The Li_2FeSiO_4 showed a maximum discharge capacity of 152.8 mAh g^{-1} and high cycling stability, while the discharge capacity of the Li_2MnSiO_4 rapidly declined

and stabilized at about 70 mAh g^{-1} after 20 cycles. Differential capacity and electrochemical impedance analysis indicated that Li_2MnSiO_4 exhibited lower electric conductivity and higher electrochemical irreversibility than those of Li_2FeSiO_4, which caused its poor electrochemical performance.

Rong *et al* [23] synthesized nanosphere like Li_2FeSiO_4–C via a solution method using sucrose as carbon sources. The cell of this sample delivered a discharge capacity of 166 mAh g^{-1} at $C/20$ rate in the first three cycles. After 30 cycles, the capacity decreased to 158 mAh g^{-1}, and the capacity retention was up to 95%. Moreover, a porous Li_2FeSiO_4–C composite consisting of nanoparticles with only 20–30 nm size, surrounded by nitrogen-doped carbon, was synthesized via a hydrothermal-assisted sol–gel method. The discharge capacity was 195.5 mAh g^{-1} at $C/10$ and 127.1 mAh g^{-1} at 5C [24]. Li_2FeSiO_4–C composite was successfully synthesized also via a refluxing-assisted solid-state reaction using ascorbic acid as an additive and sucrose as a carbon source. It delivered a discharge capacity of 163.3 mAh g^{-1} at $C/10$ [25].

Recently, Oghbaei *et al* [26] synthesized Li_2FeSiO_4 of average particle size ∼42 nm at 700°C by a citrate sol–gel method. The discharge capacity was 130 mAh g^{-1} after 30 cycles at current density $C/20$.

To the best of our knowledge, the influence of different ratios of iron to nickel in the formula $Li_2Ni_xFe_{1-x}SiO_4$ has not been investigated yet. The present work is a comprehensive study about the phase transformation, microstructure

and electrochemical performance of $Li_2Ni_xFe_{1-x}SiO_4$ samples with different Ni contents for implementation as positive electrodes in LIBs.

2. Experimental
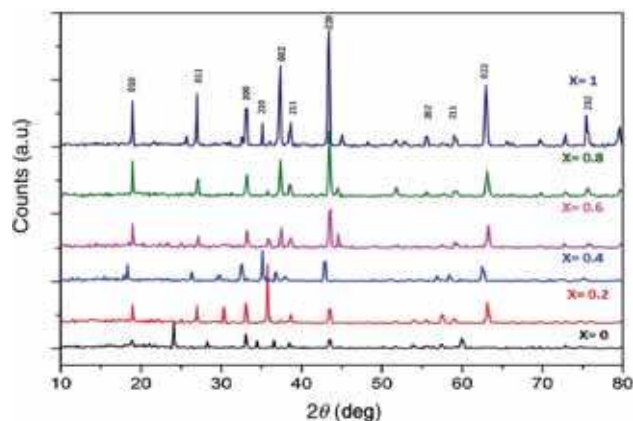
2.1 *$Li_2Ni_xFe_{1-x}SiO_4$ samples preparation*

$Li_2Ni_xFe_{1-x}SiO_4$ (x = 0, 0.2, 0.4, 0.6, 0.8 and 1) samples were prepared by a simple hydrothermal route using stoichiometric ratios weights of $LiOH·H_2O$ (98.5%, S.D., Fine), $FeC_2O_4·2H_2O$ (99%, Sigma-Aldrich), $Ni(CH_3COO)_2·4H_2O$ (99%, Sigma-Aldrich) and tetra methylsilane ($\geq$ 99%, Sigma-Aldrich) dissolved in distilled water separately in order to prepare about 5 g of each sample. The solutions of the dissolved ions were mixed together and gently heated at 80°C for 2 h to achieve high homogeneity. The mixed liquid was transferred into an autoclave with a Teflon holder inside a stainless-steel container for further heating at 200°C overnight. After cooling, the mixture was filtered and washed with distilled water and then dried at 80°C for 4 h in a vacuum oven. The dried powders were calcined at 800°C for 5 h in flowing argon gas with 5% H_2.

2.2 *Physical characterization*

The crystalline phases of calcined powders were investigated by an X-ray Brucker axis D8 diffractometer (XRD) with crystallographic data software Topas 2 using Cu-Kα (λ = 1.5406 nm) radiation operating at 40 kV and 30 mA. The angle scan rate was set at 2° min^{-1}. The microstructure and morphology of the synthesized samples were characterized by scanning electron microscopy (SEM; JOEL model 5040). Fourier transform infrared spectroscopy (FTIR) was performed using a Vector-22 (Bruker, Germany) equipment.

2.3 *Electrochemical characterization*

The working electrode (WE) was prepared from a slurry of 85% active material, 10% C-black and 5% binder (polyvinylidene difluoride: PVDF). The slurry was pasted with some drops of N-methyl pyrrolidone (NMP). An aluminium disk substrate (1 cm^2 area) was coated with this active material to form the WE. A Teflon cell was used to house the lithium foil metal (Sigma-Aldrich), which acted as counter and reference electrodes, with a separator of Celgrad (micro-porous polypropylene). The electrolyte was 1 M $LiPF_6$ dissolved in a mixture of propylene carbonate and ethylene carbonate (PC/EC = 1:1). The cells were assembled inside a glove box. Galvanostatic charging and discharging cyclings of the cells were achieved with the potentials windows between 1.5 and 4.5 V at total current 0.1 mA using a Bitrode battery tester. Furthermore, electrochemical impedance spectroscopy (EIS) measurements were performed at frequency between 10^6 and

Figure 1. XRD patterns of $Li_2Ni_xFe_{1-x}SiO_4$ (x = 0, 0.2, 0.4, 0.6, 0.8 and 1) samples prepared at 800°C.

Table 1. Crystallite size of the $Li_2Ni_xFe_{1-x}SiO_4$ (x = 0, 0.2, 0.4, 0.6, 0.8 and 1) samples.

Ni^{2+} ion content (x)	Crystallite size (nm)	a (Å)	b (Å)	c (Å)	V (Å^3)
0.0	66.08	8.213	5.012	8.226	338.611
0.2	41.29	8.218	5.018	8.231	339.429
0.4	34.76	8.223	5.020	8.230	339.729
0.6	45.28	8.211	5.016	8.227	338.840
0.8	46.67	8.189	5.011	8.222	337.390
1.0	55.30	8.036	4.997	8.199	329.238

10^{-2} Hz and an amplitude of 10 mV using a model Parastat Princeton 4000 potentiostat.

3. Results and discussion

The phase structure of prepared samples of $Li_2Ni_xFe_{1-x}SiO_4$ was characterized by XRD. The patterns are given in figure 1. The XRD pattern of Li_2FeSiO_4 sample exhibited the main peaks of monoclinic crystal system with space group $P2_1/n$; the total replacement of Fe^{2+} with Ni^{2+} ion induced a distortion into the orthorhombic unit cell with space group $Pmn2_1$ [23]. The crystallite sizes of the sample powders are calculated using the Scherer equation [3] and recorded in table 1. It is observed that $Li_2Ni_{0.4}Fe_{0.6}SiO_4$ has the smallest crystallite size, 34.76 nm. The calculated lattice cell parameters are found to be in good agreement with the previous reports [27,28].

Figure 2a–f shows SEM morphologies of $Li_2Ni_xFe_{1-x}SiO_4$ samples. The pure Li_2FeSiO_4 and Li_2NiSiO_4 exhibit large extent of agglomeration and very low porosity with particle size distribution from 10 to 40 μm. However, the Ni-substituted samples showed significant porosity and smaller particle size distribution from 100 to 1000 nm with increasing Ni content from 0.2 to 0.8. The spherical aggregates appeared
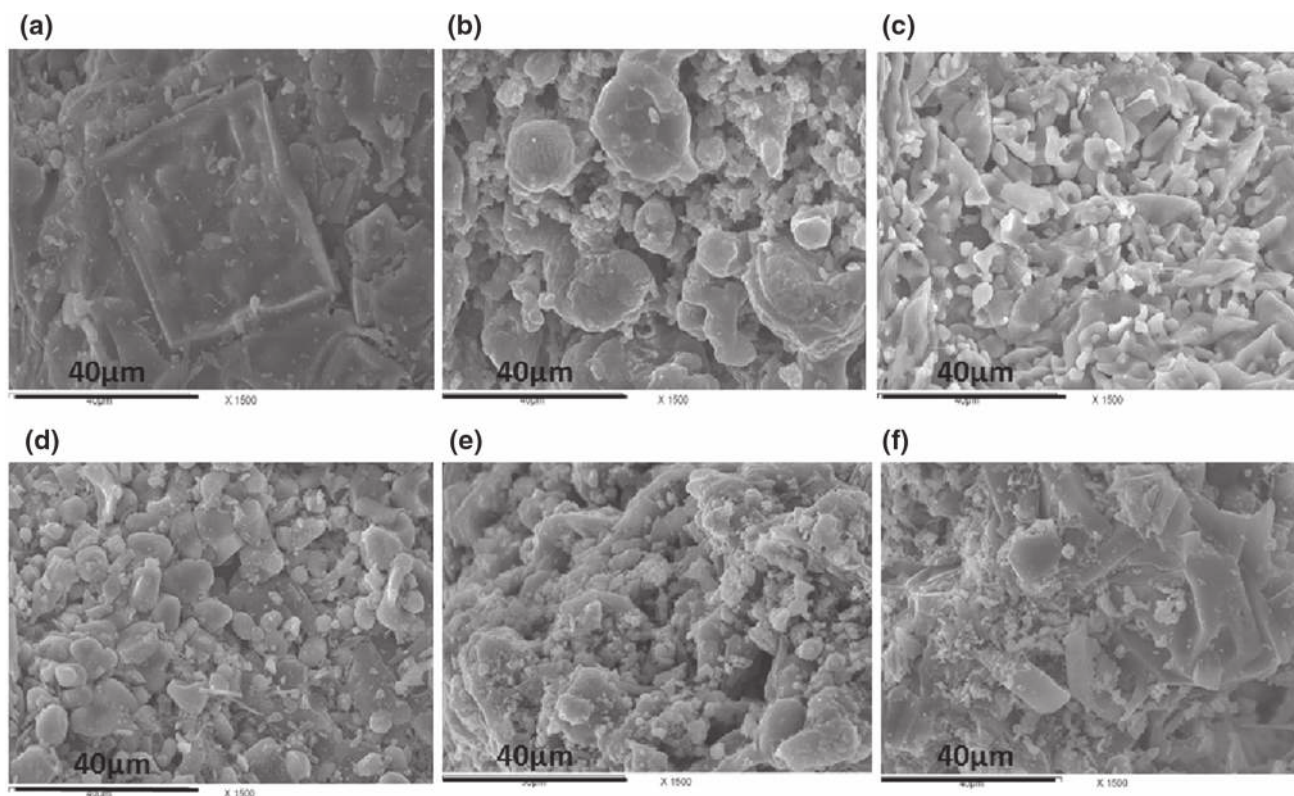
Figure 2. SEM of $Li_2Ni_xFe_{1-x}SiO_4$ ($x = 0$, 0.2, 0.4, 0.6, 0.8 and 1) samples prepared at 800°C.

as fungus-like diaspora embedded with smaller fine particles, creating large pores in the microstructure of the as-prepared materials. $Li_2Ni_{0.4}Fe_{0.6}SiO_4$ has the highest particles homogeneity and the smallest average particle size of 100–500 nm, which reflects high surface area. The average particle size from SEM micrographs are calculated using Image-Pro Software for selected areas in the sample, while the crystallite size is calculated using Scherrer's equation and XRD data. The difference between both sizes is because each particle or grain agglomerate is composed of a large number of crystals, and the formation of these particle agglomerates is controlled by many factors such as shape factor, surface area, porosity, density and electrical charge [29].

Figure 3 displays FTIR spectra of the as-prepared samples Li_2FeSiO_4 and Li_2NiSiO_4. The absorption broad bands in the wavenumber range 3800–3200 cm^{-1} could be related to the entrapped water molecule [30]. The doublet absorption band at 800 cm^{-1} is related to the monoclinic structure of Li_2FeSiO_4. The same peak splits into two stronger bands, which indicates the orthorhombic structure of Li_2NiSiO_4 [31,32]. The other characteristic absorption bands at 1455 cm^{-1} are assigned to the Li_2CO_3 formed at the surface [33].

Figure 4 reveals the first charge and discharge capacity plateaus *vs.* the working voltage between 4.5 and 1.5 V at $C/10$. It was found that the Li_2FeSiO_4 cathode gave the minimum discharge-specific capacity of ∼121 mAh g^{-1}, while
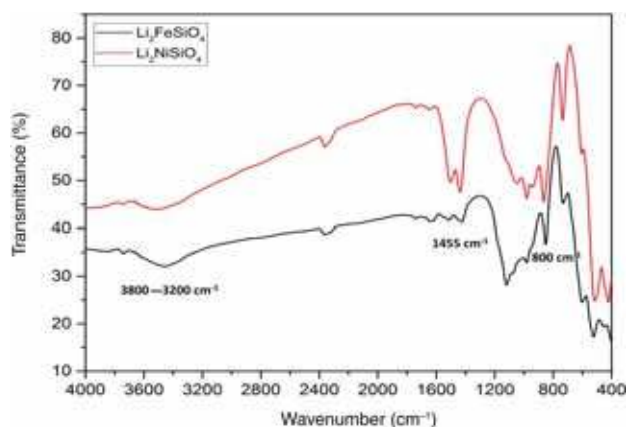

Figure 3. FTIR spectra of the as-prepared Li_2FeSiO_4 and Li_2NiSiO_4 samples.

the $Li_2Ni_{0.4}Fe_{0.6}SiO_4$ cathode material achieved the maximum discharge specific capacity of ∼164 mAh g^{-1}. This behaviour is attributed to the homogeneous morphology, regular particle size and porosity, which allows better diffusion of Li$^+$ ions and lower charge transfer resistance. The obtained results for the tested batteries are in consistent agreement with those in previous literatures [34,35].

EIS is used as a sensitive confirmation tool for studying the differences in the electrode surface behaviour and electronic
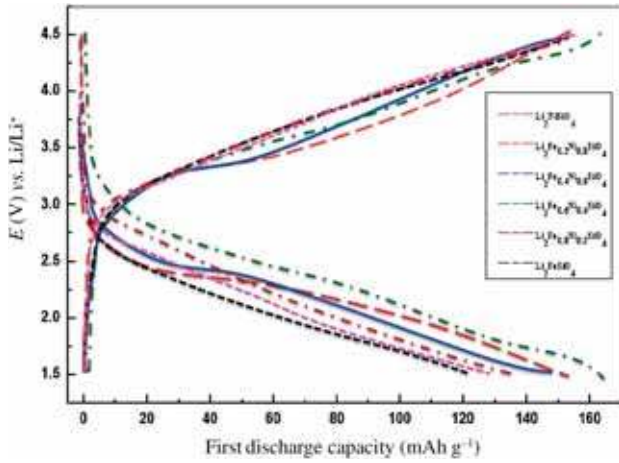
Figure 4. Voltage–capacity profiles for Li–Li$_2$Ni$_x$Fe$_{1-x}$SiO$_4$ ($x = 0, 0.2, 0.4, 0.6, 0.8$ and 1) batteries.
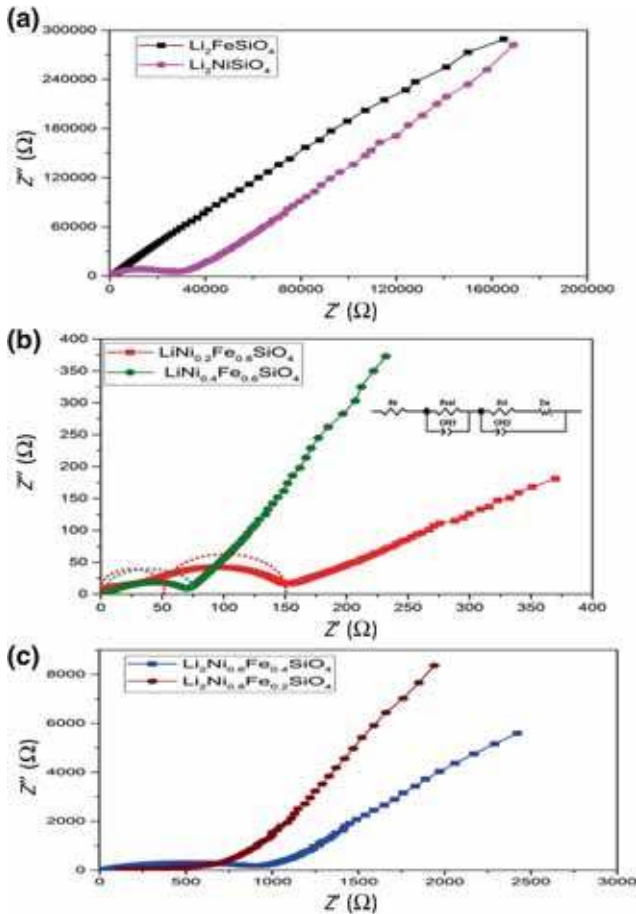
Figure 5. Nyquist plots of Li–Li$_2$Ni$_x$Fe$_{1-x}$SiO$_4$ discharged batteries after 100 cycles at (**a**) $x = 0$ and 1, (**b**) $x = 0.2$ and 0.4 and (**c**) $x = 0.6$ and 0.8.

conductivity of materials. The EIS of the discharged lithium ion batteries is illustrated by the Nyquist plot as depicted in figure 5a–c. Actually, the intercept at high frequency corresponds to the resistance of the electrolyte (R_e) on the Z_{re}

axis, followed by a semicircle in the high–middle frequency region, and a straight line in the low frequency region. The numerical value of the diameter of the semicircle on the Z_{re} axis is approximately equal to the charge transfer resistance (R_{ct}). It is observed that Li$_2$FeSiO$_4$ and Li$_2$NiSiO$_4$ cells have higher R_{ct} in comparison with the other cells. The low frequency region of the straight line is attributed to the diffusion of the lithium ions into the bulk of the electrode material, the so-called Warburg diffusion resistance. Therefore, shifting the straight lines towards smaller frequencies indicates lower diffusion of Li ions due to the solid electrolyte interface formation. It is also observed that the cells prepared from Li$_2$Ni$_{0.4}$Fe$_{0.6}$SiO$_4$ has the lowest charge transfer resistance $R_{ct} \sim 65.4\ \Omega$ in comparison with the other cells. Such a behaviour can be related to the homogeneous and good particles distribution with the smallest grain size of 2.5 μm, resulting in better diffusion of Li ions into the electrolyte. The cell volume increases with Ni substitution up to a certain composition, which improves the mobility of Li$^+$ ions through the vacancies of the orthorhombic framework.

In addition, it has been demonstrated that the doping of LiFePO$_4$ with Ni could enhance the conductivity due to the formation of percolating nano-network of metal-rich phosphide. Hence, a conductive grain boundary leads to efficient charge transfer between the bulk materials [36].

A plot of Z_{re} *vs.* the reciprocal square root of the lower angular frequencies is illustrated in figure 6a and b. The straight lines are attributed to the diffusion of the lithium ions from electrolyte into the bulk of the electrode materials, the so-called Warburg diffusion [3,8]. This relation is governed by equation (1). It is observed that the Warburg impedance coefficient (σ_w) is 269 Ω s$^{0.5}$ for Li$_2$Ni$_{0.4}$Fe$_{0.6}$SiO$_4$, which is the lowest value in comparison with the other samples as shown in figure 5b. In addition, the diffusion coefficient values of the lithium ions in the bulk electrode materials are calculated using equation (2):

$$Z_{re} = R_e + R_{ct} + \sigma_w \omega^{-0.5}, \tag{1}$$

$$D = 0.5(RT/An^2F^2\sigma_w C)^2, \tag{2}$$

where ω is angular frequency in the low frequency region, D is diffusion coefficient, R is the gas constant, T is the absolute temperature, F is Faraday's constant, A is the area of the electrode surface and C is molar concentration of Li$^+$ ions. The exchange current density is $i = RT/nFR_{ct}$). The impedance parameters of different cathode samples are presented in table 2. It is observed that Li$_2$FeSiO$_4$ has the lowest diffusion coefficient value ($\sim 1.25 \times 10^{-17}$ cm^2 s^{-1}) and Li$_2$Ni$_{0.4}$Fe$_{0.6}$SiO$_4$ has the highest diffusion coefficient value ($\sim 4.34 \times 10^{-13}$ cm^2 s^{-1}).

Figure 7 illustrates the cycle life and stability performance of the different batteries at 0.1C rate over 100 cycles. It is clearly observed that the specific discharge capacity gradually decreases in the first 10 cycles for all batteries, but sharply decreases during the subsequent 50 cycles for Li$_2$FeSiO$_4$
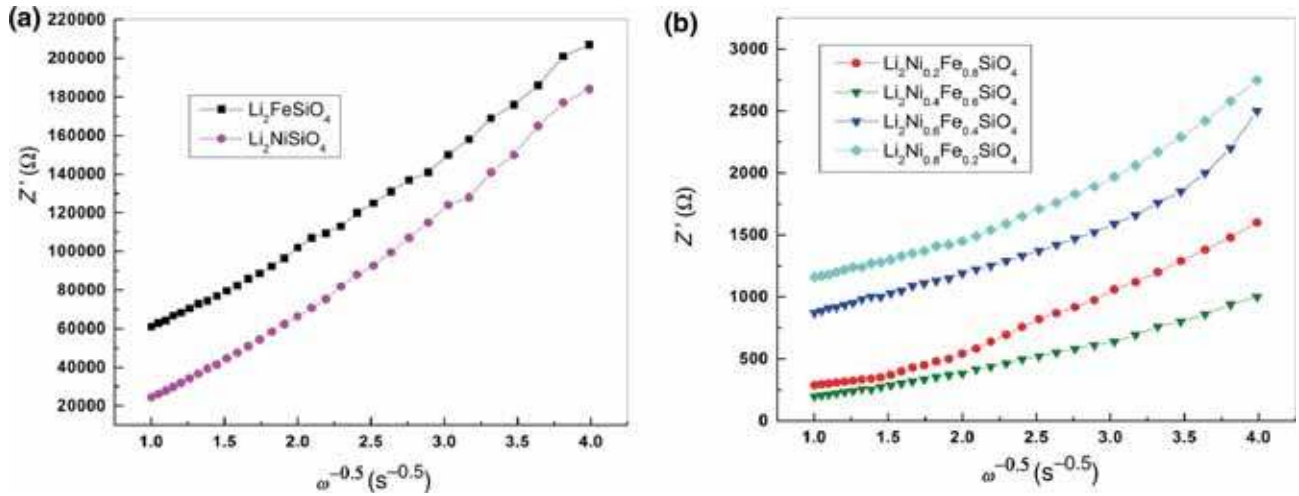
Figure 6. (**a**) Relationship between real impedance and the low angular frequencies for Li–Li_2FeSiO_4 and Li–Li_2NiSiO_4 batteries. (**b**) Relationship between real impedance and low angular frequencies for Li–$Li_2Ni_xFe_{1-x}SiO_4$ ($x = 0.2, 0.4, 0.6$ and 0.8) batteries.

Table 2. Electrochemical impedance parameters of Li–$Li_2Ni_xFe_{1-x}SiO_4$ ($x = 0, 0.2, 0.4, 0.6, 0.8$ and 1) batteries.

Cell	R_{ct} (Ω)	σ_w (Ω s$^{0.5}$)	D (cm^2 s^{-1})	C_{dl} (F)	i (A)
Li_2FeSiO_4	3.13E+04	5.33E+04	1.25E–17	9.69E–11	8.21E–07
$Li_2Ni_{0.2}Fe_{0.8}SiO_4$	1.49E+02	4.39E+02	3.80E–13	8.85E–07	1.72E–04
$Li_2Ni_{0.4}Fe_{0.6}SiO_4$	6.54E+01	2.69E+02	4.34E–13	1.85E–06	3.93E–04
$Li_2Ni_{0.6}Fe_{0.4}SiO_4$	1.52E+03	5.32E+02	1.04E–13	1.66E–07	1.70E–05
$Li_2Ni_{0.8}Fe_{0.2}SiO_4$	1.70E+03	5.45E+02	1.87E–13	5.39E–08	1.51E–05
Li_2NiSiO_4	2.55E+04	4.88E+04	1.48E–17	2.26E–09	1.01E–06
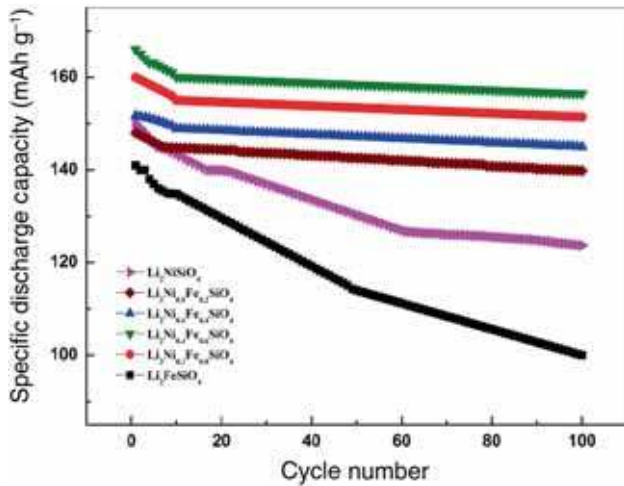
Figure 7. Cycle life performance of Li–$Li_2Ni_xFe_{1-x}SiO_4$ ($x = 0, 0.2, 0.4, 0.6, 0.8$ and 1) batteries.

and Li_2NiSiO_4 cells. This may be related to the oxidation of divalent cation Fe^{2+} to Fe^{3+} during the Li^+ diffusion. Such distortion effect in the divalent cation Fe^{2+} may affect the lattice parameters and destroy the crystallinity, leading to the noticeable capacity fading in the first 10 cycles. The greatest effect was clearly seen in pure Li_2FeSiO_4 and Li_2MnSiO_4 as reported in the literature [16,37].

The specific discharge capacity slightly decreases for $Li_2Ni_xFe_{1-x}SiO_4$ at $x = 0.2, 0.4, 0.6$ and 0.8 till 100 cycles. After 100 cycles, the $Li_2Ni_{0.4}Fe_{0.8}SiO_4$ electrode delivers the highest discharge capacity of about 156 mAh g^{-1} with coulombic efficiency of $\sim$93.9%. Thus, the cycling performance of the $Li_2Ni_xFe_{1-x}SiO_4$ cathode materials is improved with mild nickel substitution but worsened with heavy nickel substitution.

4. Conclusion

The structure of prepared samples of $Li_2Ni_xFe_{1-x}SiO_4$ was characterized by XRD. Samples are indexed on the basis of both monoclinic and orthorhombic unit cells with space groups P2$_1$/n and Pmn2$_1$, respectively. The morphological structure of materials exhibited spherical aggregated lumps with different porosities. The FTIR spectrum

analysis confirmed the phase transformation of Li_2FeSiO_4 with increasing Ni substitution. The assembled battery from $Li_2Ni_{0.4}Fe_{0.6}SiO_4$ sample showed the maximum initial discharge capacity of 164 mAh g^{-1}. It is also observed that the cell prepared from $Li_2Fe_{0.6}Ni_{0.4}SiO_4$ has the lowest real Z_{re} (charge transfer resistance: 65.4 Ω) in comparison with the other cells. Moreover, the Warburg impedance coefficient (σ_w) is 269 Ω s$^{0.5}$ for the $Li_2Ni_{0.4}Fe_{0.6}SiO_4$ cell and this is the lowest value in comparison with those of the other samples. Therefore, this cell has the maximum diffusion coefficient, 4.34E–13 cm^2 s^{-1}. Cycling performance of the $Li_2Ni_xFe_{1-x}SiO_4$ has been improved with mild nickel substitution but worsened with more nickel substitution.

References

[1] Hu M, Pang X and Zhou Z 2013 *J. Power Sour.* **237** 229

[2] Wanga X, Qinga C, Zhang Q, Fan W, Huangc X, Yanga B *et al* 2014 *Electrochim. Acta* **134** 371

[3] Shenouda A Y and Liu H K 2010 *J. Electrochem. Soc.* **157** A1183

[4] Qu L, Liu Y, Fang S, Yang L and Hirano S 2015 *Electrochim. Acta* **163** 123

[5] Shi L, Xie W, Ge Q, Wang S, Chen D, Qin L *et al* 2015 *Int. J. Electrochem. Sci.* **10** 4696

[6] Wei C, Deng J, Xi L, Zhou H, Wang Z, Chung C Y *et al* 2013 *Int. J. Electrochem. Sci.* **8** 6775

[7] Nyten A, Kamali S, Hanggstrom L, Gustafsson T and Thomas J O 2006 *J. Mater. Chem.* **16** 2266

[8] Shenouda A Y and Liu H K 2009 *J. Alloys Compd.* **477** 498

[9] Liu Y, Mi C H, Yuan C Z and Zhang X G 2009 *J. Electroanal. Chem.* **628** 73

[10] Huang H, Yin S C and Nazar L F 2004 *Electrochem. Solid-State Lett.* **4** A170

[11] Armand M, Michot C, Ravet N, Simoneau M and Hovington P 2000 US Patent 6085015

[12] Zhang S, Deng C and Yang S Y 2009 *Electrochem. Solid-State Lett.* **12** A136

[13] Dominko R, Bele M, Gaberscek M, Remskar M, Hanzel D, Pejovnik S *et al* 2006 *J. Power Sour.* **153** 274

[14] Nyten A, Abouimrane A, Armand M, Gustafsson T and Thomas J O 2005 *Electrochem. Commun.* **7** 156

[15] Zaghib K, Ait Salah A, Ravet N, Mauger A, Gendron F and Julien C M 2006 *J. Power Sour.* **160** 1381

[16] Li Y-X, Gong Z L and Yang Y 2007 *J. Power Sour.* **174** 528

[17] Zhang Q, Zhao Y, Su C and Li M 2011 *Recent Pat. Nanotechnol.* **5** 225

[18] Chen W H, Lan M, Zhu D, Wang C, Xue S, Yang C C *et al* 2013 *RSC Adv.* **3** 408

[19] Guo H, Cao X, Li X, Li L, Li X, Wang Z *et al* 2010 *Electrochim. Acta* **55** 8036

[20] Zhang S, Deng C, Fu B L, Yang S Y and Ma L 2010 *Electrochim. Acta* **55** 8482

[21] Zhang L-L, Sun H B, Yang X L, Wen Y W, Huang Y H, Li M *et al* 2015 *Electrochim. Acta* **152** 496

[22] Deng C, Zhang S, Fu B L, Yang S Y and Ma L 2010 *Mater. Chem. Phys.* **120** 14

[23] Rong Y, Xiaoyan L, Ye Q, Jing L and Ahn J H 2012 *Trans. Nonferrous Met. Soc. China* **22** 2529

[24] Zhang Z, Liu X, Wang L, Wu Y, Zhao H and Chen B 2015 *Solid State Ion.* **276** 33

[25] Li M, Zhang L-L, Yang X L, Huang Y H, Sun H B, Ni S B *et al* 2015 *J. Solid State Electrochem.* **19** 415

[26] Oghbaei M, Baniasadi F and Asgari S 2016 *J. Alloys Compd.* **672** 93

[27] Zhong G, Li Y, Yan P, Liu Z, Xie M and Lin H 2010 *J. Phys. Chem. C* **114** 3693

[28] Zhang L, Duan S, Yang X, Liang G, Huang Y, Cao X *et al* 2015 *J. Mater. Chem. A* **3** 6004

[29] Sanad M M S, Rashad M M, Abdel-Aal E A, El-Shahat M F and Powers K 2014 *J. Mater. Sci.: Mater. Electron.* **25** 2487

[30] Sanad M M S, Rashad M M, Abdel-Aal E A, El-Shahat M F and Powers K 2014 *J. Rare Earths* **32** 37

[31] Luo S H, Wang M, Zhu X and Geng G H 2012 *Key Eng. Mater.* **512–515** 1588

[32] Pandey M, Ramar V, Balaya P and Kshirsagar R J 2015 *AIP Conf. Proc.* **1665** 140044-1

[33] Jaén J A, Iglesias J, Muñoz A, Tabares J A and Pérez Alcázar G A 2015 *Croat. Chem. Acta* **88** 487

[34] Kojima T, Okuyama Y, Kojima A, Sakai T and Miyuki T 2011 *J. Electrochem. Soc.* **158** A1340

[35] Xu Y, Shen W, Zhang A, Liu H and Ma Z 2014 *J. Mater. Chem. A* **2** 12982

[36] Herle P S, Ellis B, Coombs N and Nazar L F 2004 *Nat. Mater.* **3** 147

[37] Nyten A, Kamali S, Haggstrom L, Gustafsson T and Thomas J O 2006 *J. Mater. Chem.* **16** 2266